

# The SAMI Galaxy Survey: Detection of Environmental Dependence of Galaxy Spin in Observations and Simulations Using Marked Correlation Functions

TOMAS H. RUTHERFORD,<sup>1,2</sup> SCOTT M. CROOM,<sup>1,2</sup> JESSE VAN DE SANDE,<sup>1,2</sup> CLAUDIA DEL P. LAGOS,<sup>3,2</sup>  
JOSS BLAND-HAWTHORN,<sup>1,2</sup> S. BROUGH,<sup>4,2</sup> JULIA J. BRYANT,<sup>1,5,2</sup> FRANCESCO D'EUGENIO,<sup>6</sup> AND MATT S. OWERS<sup>7,8</sup>

<sup>1</sup>*Sydney Institute for Astronomy, School of Physics, A28, The University of Sydney, NSW, 2006, Australia*

<sup>2</sup>*ARC Centre of Excellence for All Sky Astrophysics in 3 Dimensions (ASTRO 3D), Australia*

<sup>3</sup>*International Centre for Radio Astronomy Research (ICRAR), M468, University of Western Australia, 35 Stirling Hwy, Crawley, WA 6009, Australia*

<sup>4</sup>*School of Physics, University of New South Wales, NSW 2052, Australia*

<sup>5</sup>*Australian Astronomical Optics, AAO-USydney, School of Physics, University of Sydney, NSW 2006, Australia*

<sup>6</sup>*Sterrenkundig Observatorium, Universiteit Gent, Krijgslaan 281 S9, B-9000 Gent, Belgium*

<sup>7</sup>*Department of Physics and Astronomy, Macquarie University, NSW 2109, Australia*

<sup>8</sup>*Astronomy, Astrophysics and Astrophotonics Research Centre, Macquarie University, Sydney, NSW 2109, Australia*

(Accepted June 25, 2021)

Submitted to ApJ

## ABSTRACT

The existence of a kinematic morphology-density relation remains uncertain, and instead stellar mass appears the more dominant driver of galaxy kinematics. We investigate the dependence of the stellar spin parameter proxy  $\lambda_{R_e}$  on environment using a marked cross-correlation method with data from the SAMI Galaxy Survey. Our sample contains 710 galaxies with spatially resolved stellar velocity and velocity dispersion measurements. By utilising the highly complete spectroscopic data from the GAMA survey, we calculate marked cross-correlation functions for SAMI galaxies using a pair count estimator and marks based on stellar mass and  $\lambda_{R_e}$ . We detect an anti-correlation of stellar kinematics with environment at the  $3.2\sigma$  level, such that galaxies with low  $\lambda_{R_e}$  values are preferably located in denser galaxy environments. However, a significant correlation between stellar mass and environment is also found (correlation at  $2.4\sigma$ ), as found in previous works. We compare these results to mock-observations from the cosmological EAGLE simulations, where we find a similar significant  $\lambda_{R_e}$  anti-correlation with environment, and a mass and environment correlation. We demonstrate that the environmental correlation of  $\lambda_{R_e}$  is not caused by the mass-environment relation. The significant relationship between  $\lambda_{R_e}$  and environment remains when we exclude slow rotators. The signals in SAMI and EAGLE are strongest on small scales (10-100 kpc) as expected from galaxy interactions and mergers. Our work demonstrates that the technique of marked correlation functions is an effective tool for detecting the relationship between  $\lambda_{R_e}$  and environment.

*Keywords:* Two-point correlation function (1951), Galaxy Surveys (1378)— Galaxy Kinematics (602)  
— Galaxy Environments (2029) — Galaxy Clustering (584)

## 1. INTRODUCTION

A relationship exists between galaxy properties and local environmental density (Dressler 1980), such that early-type galaxies (ETGs) are preferably found in denser environments. Although the kinematic proper-

ties of galaxies do not correlate one-to-one with visual morphology, a tentative relationship between a proxy for the spin parameter,  $\lambda_{R_e}$ , and environmental density was presented by Cappellari et al. (2011). This kinematic morphology-density relation (KMDR) suggests that the fraction of slow rotating galaxies (low  $\lambda_{R_e}$ ) increases towards denser environments. However, galaxy stellar mass also correlates with both environment and the in-

intrinsic properties of galaxies. Thus, the question arises what the true physical driver of the KMDR is.

Further work supported the picture of a KMDR (D'Eugenio et al. 2013; Houghton et al. 2013; Scott et al. 2014; Fogarty et al. 2014). More recent results with larger galaxy samples find that the KMDR is driven mostly by stellar mass (Brough et al. 2017; Veale et al. 2017; Greene et al. 2017), but that the KMDR may also still exist at fixed stellar mass (Graham et al. 2019). There is also evidence from simulations that points towards environmental dependence as a weaker secondary effect, but mass as the primary physical driver (e.g. Lagos et al. 2017). Some clear results have emerged, i.e. the trend with mass, but it is evident that any environmental dependence is likely to be a second order effect.

Multi-object integral field spectroscopy has revolutionised the number of galaxies with spatially resolved kinematic measurements. The Sydney-Australian-Astronomical-Observatory Multi-object Integral-Field Spectrograph (SAMI) galaxy survey has observed  $\sim 3000$  galaxies (Croom et al. 2012), while the Mapping Nearby Galaxies at Apache Point Observatory (MaNGA) survey aims to observe  $\sim 10,000$  galaxies (Bundy et al. 2015). Other ancillary surveys such as the Sloan Digital Sky Survey (SDSS; York et al. 2000) and the Galaxy and Mass Assembly Survey (GAMA; Driver et al. 2011) enable an accurate definition of environment, tracing the underlying large scale structure that exists in the Universe.

With the growing wealth of spatially resolved kinematic data, the statistical tool of correlation functions becomes more powerful. It allows us to connect large scale structure in galaxy clustering to internal galaxy properties, in our case galaxy spin, parameterised by  $\lambda_{R_e}$ . Correlation functions have already demonstrated a relation between environment and the star-forming and morphological properties of galaxies (e.g. Madgwick et al. 2003; Hermit et al. 1996). Marked correlation functions, where galaxies are marked by some physical parameter, are even more effective at detecting and quantifying weak correlations with environment (Sheth & Tormen 2004; Harker et al. 2006), making this method ideal for detecting a possible relation between  $\lambda_{R_e}$  and environment.

Most papers look at the fraction of fast and slow rotators as a function of mass and environment (Cappellari et al. 2011; Brough et al. 2017; Veale et al. 2017; Greene et al. 2017; Graham et al. 2019), whereas a broader analysis of the  $\lambda_{R_e}$  distribution as a function of mass and environment shows that environment might have a small impact on  $\lambda_{R_e}$  (Wang et al. 2020).

In this paper we aim to investigate the correlation between  $\lambda_{R_e}$  and environmental density. We present an analysis using marked cross correlation functions applied to SAMI (Croom et al. 2012) and GAMA (Driver et al. 2011) data, as well as mock observations from the EAGLE Simulations (Schaye et al. 2015). We adopt a  $\Lambda$ CDM cosmology, with  $H_0 = 70 \text{ km s}^{-1} \text{ Mpc}^{-1}$ ,  $\Omega_m = 0.3$ ,  $\Omega_\Lambda = 0.7$ .

## 2. OBSERVATIONS AND SIMULATIONS

### 2.1. Observations

The SAMI instrument (Croom et al. 2012) is mounted on the Anglo-Australian Telescope and provides a 1 degree diameter field of view. SAMI employs 13 fused fibre bundles (Hexabundles; Bland-Hawthorn et al. 2011; Bryant et al. 2014) with a high (75%) fill factor. Each bundle contains 61 fibres of 1.6" diameter resulting in each IFU having a diameter of 15 ". The IFUs, as well as 26 sky fibres, are fed to the AAOmega spectrograph (Sharp et al. 2006), using the 580V grating at 3570-5750Å giving a resolution of  $R=1808$  ( $\sigma=70.4 \text{ km s}^{-1}$ ), and the R1000 grating from 6300-7400Å giving a resolution of  $R=4304$  ( $\sigma=29.6 \text{ km s}^{-1}$ ) (van de Sande et al. 2017a).

The SAMI Galaxy survey (Croom et al. 2012; Bryant et al. 2015) selected galaxies from the GAMA (Driver et al. 2011) survey, in addition to eight low-redshift clusters (Owers et al. 2017). Reduced data cubes (Sharp et al. 2015) and stellar kinematic maps are available with the SAMI Galaxy Survey data releases (Allen et al. 2015; Green et al. 2018; Scott et al. 2018; Croom et al. 2021).

Our sample contains 1832 galaxies with  $\lambda_{R_e}$  measurements, derived from spatially resolved kinematic measurements as described in van de Sande et al. (2017a), and include an aperture correction (van de Sande et al. 2017b) and a seeing correction (Harborne et al. 2020; van de Sande et al. 2020). Furthermore, we define a volume-limited sample by selecting galaxies at: 1)  $z < 0.06$  to avoid biases in the marked correlation function as the SAMI selection function results in different distributions of galaxy stellar masses in different volumes, and 2)  $M/M_\odot > 10^{10}$  to avoid low-completeness in the stellar kinematic sample. Alternatively, we could have treated each redshift section within the SAMI function selection individually, and taken a variance weighted mean of each resulting correlation function. While this achieves a stronger signal, the result becomes more difficult to interpret due to our ranking method for weights (Section 3). The final sample contains 710 galaxies, of all morphological types. This sample is unique amongst other similar surveys. For example, ATLAS<sup>3D</sup>'s sam-

ple for kinematic analysis (Cappellari et al. 2011) only contained 260 field ETGs, and MaNGA (10,000 galaxies, Bundy et al. 2015) is only a narrow band in the mass redshift plane, with a complicated selection function that may make analyses that require volume limited samples more difficult to replicate.

Galaxies from the GAMA survey (Driver et al. 2011; Liske et al. 2015) serve as a background galaxy distribution for our analysis. GAMA adopted an r-band magnitude limit of  $r_{\text{pet}} < 19.8$  mag. For our analysis, we restrict the GAMA sample at  $z < 0.06$  ( $z_{\text{max}}$  of SAMI) and define a volume-limited sample in redshift and r-band apparent magnitude. This was done so that the background distribution was not biased by a higher density of fainter galaxies at lower redshifts in an apparent magnitude limited sample. The GAMA data used in this paper came from three equatorial regions centred at  $9^h$ ,  $12^h$  and  $14.5^h$  in RA, each of  $12 \times 4$  deg<sup>2</sup>.

## 2.2. Simulations

We use galaxy mock-observations from the EAGLE hydrodynamical cosmological simulation suite (Schaye et al. 2015) as presented by Lagos et al. (2018). A total of  $7 \times 10^8$  galaxies were extracted from the 100 Mpc<sup>3</sup> box, where each baryonic particle has an initial mass of  $1.8 \times 10^6 M_{\odot}$ , with a maximum gravitational softening length of 0.7 kpc. We adopt a stellar mass cut of  $M_{\text{stars}} > 5 \times 10^9 M_{\odot}$ , to ensure galaxies had angular momentum profiles that converged.  $\lambda_{R_e}$  values were derived for mock-observations of this sample, leaving us with 5587 galaxies. A sample of 29737 galaxies not subjected to the stellar mass cut serves as the background galaxy distribution. These samples have an effective mass limit of  $M/M_{\odot} > 10^{8.5}$ .

Additionally, as the mass distributions of SAMI and EAGLE galaxies are significantly different, we use a set of galaxies sampled from EAGLE in such a way to match the SAMI mass distribution. The initial distributions can be seen in Figure 1.

## 3. MARKED CORRELATION FUNCTIONS

Marked statistics are a powerful tool to determine whether correlations between galaxy parameters depend on environment or not. Galaxies are assigned a mark, corresponding to some physical parameter, and a marked correlation function (Sheth & Tormen 2004; Sheth et al. 2005) is calculated. We begin by defining the 2-point real-space correlation function  $\xi(r)$ , given by Peebles (1980):

$$dP = \rho^2 [1 + \xi(r)] dV_1 dV_2, \quad (1)$$

where  $dP$  is the probability for two galaxies to be located at a distance  $r$  from each other, in volume elements  $dV_1$

and  $dV_2$ .  $\rho$  is the mean density of galaxies in the volume considered. The correlation function  $\xi(r)$  measures the ‘‘overdensity’’ of galaxies. In our case, we assume that redshift gives the radial distance to a galaxy. This is known as a redshift-space ( $s$ ) correlation function,  $\xi(s)$ .

In practice, estimators are used to calculate  $\xi(s)$ . We use an estimator introduced by Peebles (1980):

$$1 + \xi(s) = \frac{\langle SG(s) \rangle}{\langle SG_R(s) \rangle}, \quad (2)$$

where  $\langle SG(s) \rangle$  and  $\langle SG_R(s) \rangle$  are pair counts between a SAMI ( $S$ ) and GAMA ( $G$ ) galaxy, and a SAMI and random GAMA ( $G_R$ ) galaxy respectively. These pair counts are calculated by first defining radial bins, equally spaced in  $\log_{10}(s)$ . A SAMI galaxy is selected, and the distance to each GAMA galaxy is calculated. A count is then added to each relevant radial bin. This is repeated for all SAMI galaxies. Random GAMA galaxies are a sample of GAMA-like galaxies, created in such a way to match GAMA’s selection function.

We now assign SAMI galaxies marks ( $m$ ). Galaxies are ranked in  $\lambda_{R_e}$  and log stellar mass, with the mark taken as the rank, to ensure an equivalent dynamical range for both marks. Marked correlation functions can then be thought of as a ratio of galaxy marks to the mean mark,  $\bar{m}$ , as a function of galaxy separation (Sheth et al. 2005):

$$\begin{aligned} M(s) &\equiv \frac{\sum m(\mathbf{x})m(\mathbf{y})\mathcal{I}(|\mathbf{x} - \mathbf{y}| - s)}{\bar{m}_x \bar{m}_y \sum \mathcal{I}(|\mathbf{x} - \mathbf{y}| - s)} \\ &= \frac{\sum m(\mathbf{x})\mathcal{I}(|\mathbf{x} - \mathbf{y}| - s)}{\bar{m}\rho^2[1 + \xi(s)]}, \end{aligned} \quad (3)$$

where  $m(\mathbf{x})$  is the mark of a SAMI galaxy. We have defined the mark of all GAMA galaxies [ $m(\mathbf{y})$ ] to be 1,  $\mathcal{I}(x) = 0$  unless  $x = 0$ , and the sum is over all SAMI-GAMA galaxy pairs. As we have divided by  $\bar{m}$ ,  $M(s) = 1$  for all  $s$  if no correlation between marks and environment exists.

We can also consider Equation 3 in an alternate way. By a simple re-arrangement, the denominator can be expressed as one plus the regular correlation function, defined in Equation 1, and the numerator as one plus a ‘‘weighted’’ correlation function. This weighted correlation function, defined as  $W(s)$ , can be calculated using the same estimator as  $\xi(s)$ , except the  $i^{\text{th}}$  SAMI galaxy contributes a weight of  $m_i/\bar{m}$  to the relevant radial bins:

$$\begin{aligned} M(s) &\equiv \frac{\sum (m(\mathbf{x})/\bar{m})\mathcal{I}(|\mathbf{x} - \mathbf{y}| - s)}{\sum \mathcal{I}(|\mathbf{x} - \mathbf{y}| - s)} \equiv \frac{1 + W(s)}{1 + \xi(s)} \\ &= \frac{\langle WG(s) \rangle}{\langle SG(s) \rangle}, \end{aligned} \quad (4)$$

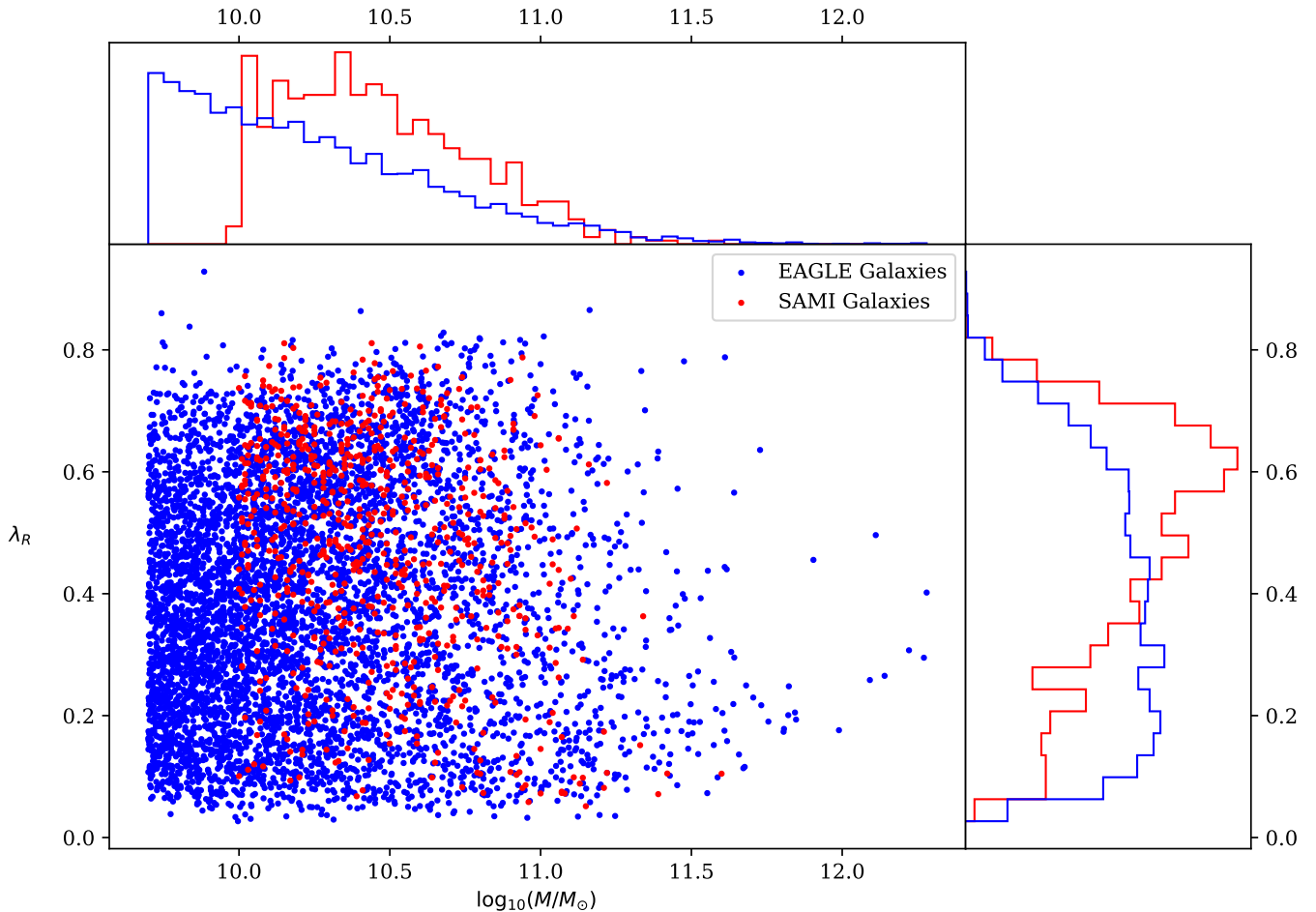


**Figure 1.** The distribution of SAMI (red) and EAGLE (blue) galaxies in  $\log_{10}(M/M_{\odot})$ - $\lambda_{R_e}$  space. The normalised histograms of both samples for both parameters is also included. In this paper we adopt a mass limit for SAMI of  $\log_{10}(M/M_{\odot}) > 10$ .

where  $\langle WG(s) \rangle$  are *weighted* pair counts between weighted SAMI ( $W$ ) and GAMA ( $G$ ) galaxies, and  $\langle SG(s) \rangle$  are *unweighted* pair counts between SAMI ( $S$ ) and GAMA galaxies. Marked correlation functions with random marks are also calculated, as a check that any signal seen in the real functions is legitimate. Once our correlation functions are calculated, we use the Python emcee package (Foreman-Mackey et al. 2013) to fit a function of the form:

$$M(s) = 1 + As^{-m} \quad (5)$$

We use this functional form as we expect  $M(s) \approx 1$  for all scales other than small scales, where it may deviate according to possible spin-environment and mass-environment relations. Uncertainties are calculated from the 16<sup>th</sup> and 84<sup>th</sup> percentiles.

### 3.1. Uncertainty Calculation

We choose bootstrap re-sampling for our uncertainty estimate, as bootstrap re-sampling is robust and as

shown by Fisher et al. (1994), at worst overestimates error in correlation functions. Importantly, bootstrap uncertainties assume zero correlation between points, which is not strictly true in our case, as single galaxies contribute to multiple pair counts. However, on small scales the data points are largely independent, due to the small number of galaxies contributing to pairs at such small separation. As another test, we also evaluated another two different error estimations. We divided our sample into nine regions, and calculated a correlation function in each region, taking the standard deviation between the regions. We also calculated Poissonian errors for each bin. We found that the bootstrap errors were similar to Poissonian at small scales, and similar to the nine region standard deviation at large scales. Due to this, and our largely independent points at small scales, we use ordinary bootstrap re-sampling as a close approximation of errors.

As bootstrap re-sampling generally overestimates uncertainties at small scales by a factor  $\sqrt{3}$  (Croom &

Shanks 1996), the number of SAMI galaxies drawn per bootstrap sample was  $3N$ , where  $N$  is the total number of galaxies, as also suggested by Norberg et al. (2001). Previous galactic correlation function works have used 10 re-samples (Hermit et al. 1996) or 20 re-samples (Madgwick et al. 2003). Due to our smaller data set in SAMI, we created 10,000 re-samples for each correlation function.

## 4. RESULTS

### 4.1. SAMI Galaxies

We present marked correlation functions for SAMI Galaxies, with ranked  $\lambda_{R_e}$  and stellar mass marks, in Figure 2.

Towards small scales  $s$  we find that the marked correlation measurements (orange symbols) are significantly less than 1, i.e., there is a significant anti-correlation of ranked  $\lambda_{R_e}$  with environment. The best-fit power-law (Equation 5, Figure 2a, red line), shows a significant turn below  $M(s) = 1$ , beginning at around  $s = 1$  Mpc. We find a best-fit value for  $A = -0.038^{+0.012}_{-0.013}$ ,  $3.2\sigma$  below zero. This implies that galaxies with low  $\lambda_{R_e}$  start being preferentially located in dense environments at scales of  $s \approx 1$  Mpc. As done by Harker et al. (2006), we also take one large radial bin out to 1 Mpc to find significance at small scales ( $M(< 1Mpc)$ ). We find  $M(< 1Mpc) = 0.925 \pm 0.034$ ,  $2.2\sigma$  below 1. Randomised marks are consistent with  $M(s) = 1$  at all scales.

In Figure 2b we also detect a significant correlation of ranked stellar mass with environment. The best-fit power-law (red line) shows a significant up turn above  $M(s) = 1$  towards small scales in  $s$ , beginning at around  $s = 1$  Mpc. We find a best-fit value of  $A = 0.036^{+0.015}_{-0.015}$ ,  $2.4\sigma$  above zero. This result implies that galaxies with high stellar mass start being preferentially located in dense environments at scales of  $\approx 1$  Mpc. We find  $M(< 1Mpc) = 1.058 \pm 0.042$ ,  $1.4\sigma$  above zero. This result is consistent with previous work, as galaxies are well known to cluster according to mass (or luminosity) (e.g. Norberg et al. 2002). Randomised marks are consistent with  $M(s) = 1$  at all scales.

#### 4.1.1. Further Analysis of SAMI Results

We have found an anti-correlation of  $\lambda_{R_e}$  with environment, and a positive correlation of stellar mass with environment. We can compare these results with different tests. First, we reverse the rank order for  $\lambda_{R_e}$  and compare  $M(< 1Mpc)$  for these reverse  $\lambda_{R_e}$  ranks and stellar mass ranks. We find  $M(< 1Mpc) = 1.075 \pm 0.043$  for reverse  $\lambda_{R_e}$  and  $M(< 1Mpc) = 1.058 \pm 0.041$  for stellar mass. This gives a difference of  $0.017 \pm 0.059$ . Using this metric, mass and reverse  $\lambda_{R_e}$  rank marks

are consistent. However, this simplistic approach of assuming a one-to-one relationship between reversed  $\lambda_{R_e}$  ranks and stellar mass ranks is not entirely supported, as there is a lot of scatter in this relationship (Croom et al. 2021). In Figure 3, we present two methods of testing for the physical driver of our SAMI  $\lambda_{R_e}$ -environment anti-correlation. Bins are defined in stellar mass of 0.1 dex in width. Galaxies are then assigned a  $\lambda_{R_e}$  value from another random galaxy in their mass bin. This failed to reproduce a negative correlation with environment. The lack of correlation in this case implies that the signal we see between  $\lambda_{R_e}$  and environment cannot be caused purely by a mass-environment relation. Removing slow rotators ( $\lambda_{R_e} < 0.2$ ) from the sample did reproduce a negative correlation with environment. This existence of a correlation implies that the observed correlation between  $\lambda_{R_e}$  and environment cannot be attributed solely to slow rotators.

### 4.2. EAGLE Galaxies

We show the distribution in  $\lambda_{R_e}$  and stellar mass of SAMI and EAGLE galaxies in Figure 1. As the mass distributions are significantly different, we create a set of observations sampled from EAGLE in such a way to match the SAMI mass distribution. Fifty bins spaced in  $\log(M/M_\odot)$  were defined across the mass range for SAMI, and EAGLE galaxies in each bin were drawn randomly until there were three times as many EAGLE galaxies in each bin as SAMI.

We present marked correlation functions for these re-sampled EAGLE galaxies, with ranked  $\lambda_{R_e}$  and stellar mass marks, in Figure 4. We see a significant anti-correlation of ranked  $\lambda_{R_e}$  with environment in our marked correlation function for EAGLE (Figure 4a). The best-fit power-law shows a significant downward trend towards small scales in  $s$ .  $m$  is lower for EAGLE than for SAMI, so the correlation between  $\lambda_{R_e}$  and environment extends to larger scales in EAGLE than in SAMI. We find a best-fit value of  $A = -0.020^{+0.003}_{-0.003}$ ,  $6.6\sigma$  below zero. This implies that in the EAGLE mock-observations, low- $\lambda_{R_e}$  galaxies are preferentially located in dense environments, out to scales of the order  $\sim 1$  Mpc. This is consistent with our SAMI results. We find  $M(< 1Mpc) = 0.966 \pm 0.008$ ,  $4.2\sigma$  below 1. Randomised marks are consistent with  $M(s) = 1$  at all scales.

We see a significant correlation of ranked stellar mass with environment in our marked correlation function for EAGLE. The best-fit power-law shows a significant upwards trend towards small scales in  $s$ . We find a best fit value of  $A = 0.030^{+0.003}_{-0.003}$ ,  $10\sigma$  above zero. This implies that in the EAGLE mock-observations, high stellar mass galaxies are preferentially located in dense envi-

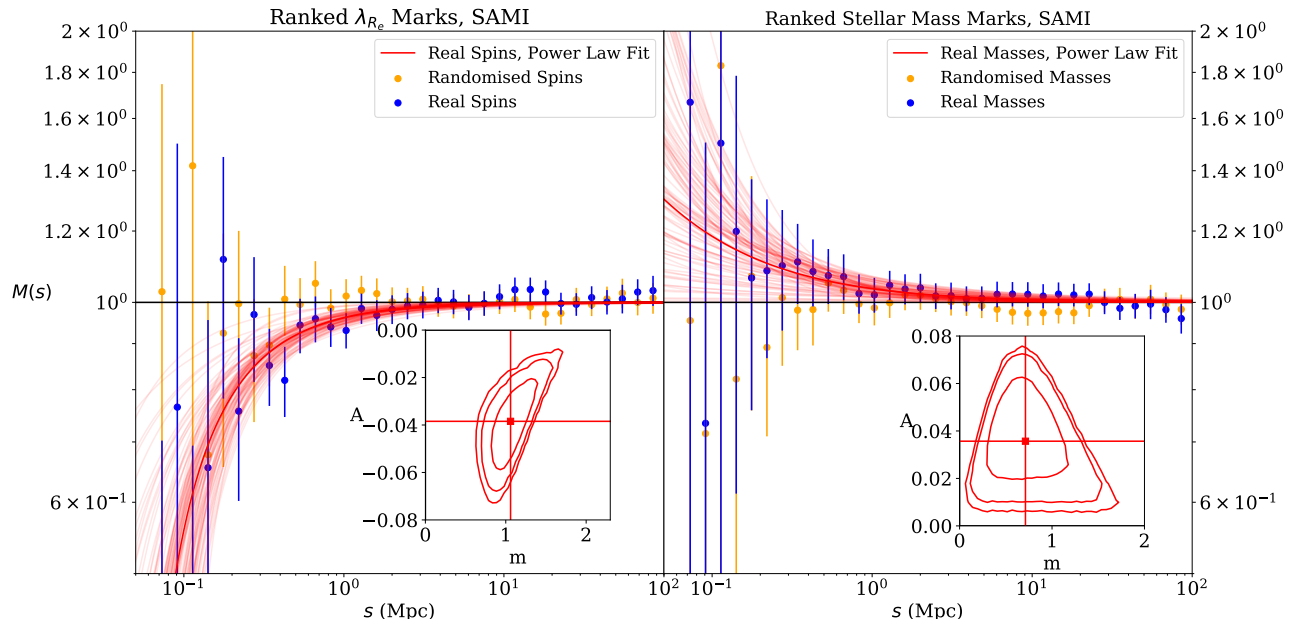


**Figure 2.** Marked correlation functions for ranked  $\lambda_{Re}$  (left panel) and ranked stellar mass marks (right panel), with SAMI galaxies (blue data). Randomised marks are plotted as a test of our method (orange data). We plot the best-fit power law (dark red line). One hundred samples from the MCMC chain (light red lines) are plotted, as a representation of the uncertainty in the fits. Contours for the 68<sup>th</sup>, 90<sup>th</sup> and 95<sup>th</sup> percentiles are plotted for the real data in  $A$  and  $m$  space, as explored by the emcee algorithm, in the inset. The red overlay lines in these parameter spaces represent the values of  $A$  and  $m$  selected at the 50<sup>th</sup> percentile. Measures of the significance can be found in Table 1.  $\lambda_{Re}$  is negatively correlated with environment, while stellar mass is positively correlated with environment in SAMI galaxies.

ronments, out to scales of the order  $\sim 10$  Mpc. We find  $M(< 1\text{Mpc}) = 1.066 \pm 0.015$ ,  $4.4\sigma$  above 1. Randomised marks are consistent with  $M(s) = 1$  at all scales, as expected.

## 5. CONCLUSION

We investigate the existence of a kinematic morphology-density relation (KMDR) using the technique of marked correlation functions. Ranking galaxies by their spin (parametrised by  $\lambda_{Re}$ ) and stellar mass allows us to investigate whether the relation is driven purely by stellar mass or if some residual spin correlation exists. This is the first time that marked correlation functions have been applied to galactic spin. We apply our analysis to both the SAMI observations and EAGLE simulation mock-observations, allowing us to compare SAMI to simulated results. The GAMA dataset is used as the “background” in the SAMI analysis for measuring large scale structure, due to GAMA’s highly complete spectroscopic data. We estimate uncertainties in all our correlation functions through bootstraps with 10,000 re-samples, and estimate significance by fitting power laws of the form  $M(s) = 1 + As^{-m}$  and looking at single bins below 1 Mpc.

We find the following results:

- Mass is positively correlated with environment. Fitting our ranked mass mark correlation function by a power law gave parameters  $A = 0.036^{+0.015}_{-0.015}$ , and  $m = 0.713^{+0.320}_{-0.255}$ . These results are consistent with previous work (e.g. Norberg et al. 2002).
- Spin (parametrised by  $\lambda_{Re}$ ) is negatively correlated with environment. Fitting our ranked  $\lambda_{Re}$  mark correlation function by a power law gave parameters  $A = -0.038^{+0.012}_{-0.013}$ , and  $m = 1.060^{+0.196}_{-0.179}$ . This is consistent with previous work that found evidence of a KMDR (Cappellari et al. 2011; D’Eugenio et al. 2013; Houghton et al. 2013; Scott et al. 2014; Fogarty et al. 2014), and the presence of an environmental effect on spin (Choi et al. 2018).
- Spin anti-correlation with environment is not driven solely by stellar mass. Defining bins in stellar mass of 0.1 dex, galaxies are assigned random  $\lambda_{Re}$  values corresponding to their mass bin. This failed to reproduce a negative correlation with environment.

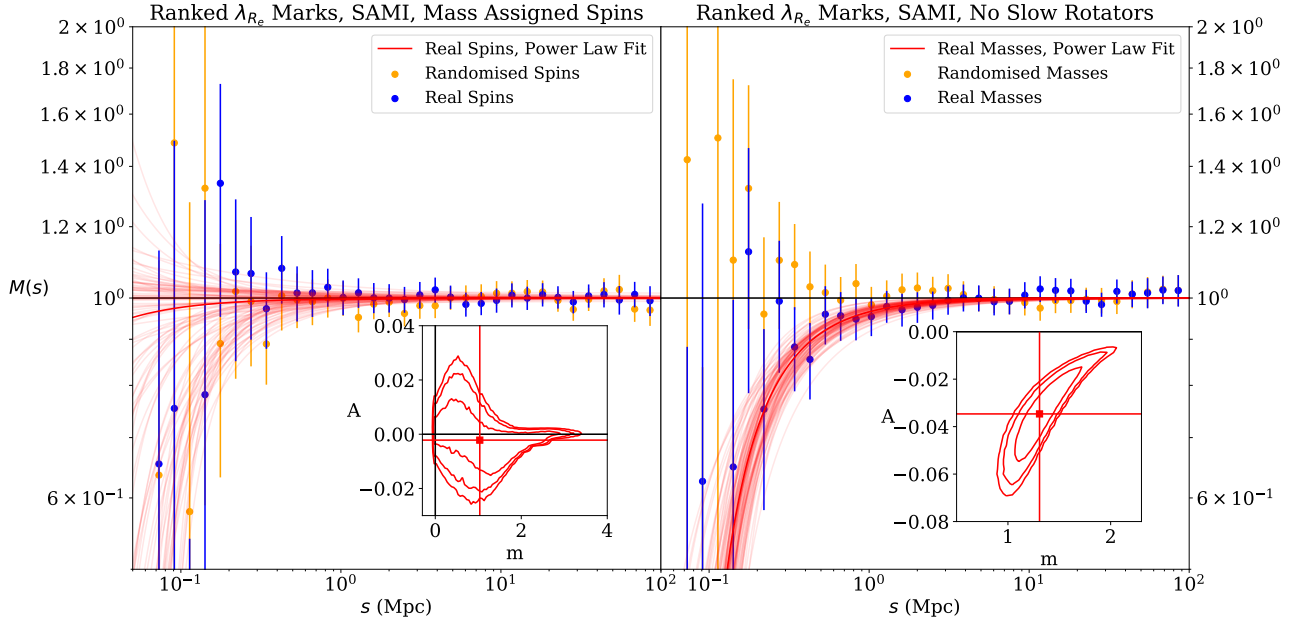


**Figure 3.** Marked correlation functions for different tests exploring whether our SAMI  $\lambda_{R_e}$  anti-correlation with environment can be explained by mass trends. Selecting a galaxy’s  $\lambda_{R_e}$  value at random from 0.1 dex mass bins failed to reproduce a negative correlation (left panel). Removing slow rotators from the SAMI sample ( $\lambda_{R_e} < 0.2$ ) still reproduces a negative correlation (right panel). Randomised marks are also plotted as a test of our method. Symbols and lines are similar as in Figure 2, but now presented for mass-defined  $\lambda_{R_e}$  and for a sample with slow rotators removed. The anti-correlation of  $\lambda_{R_e}$  with environment is not driven purely by stellar mass, or by slow rotators.

**Table 1.** Measurements of the significance of the signals in the correlation functions for SAMI and EAGLE data. We present the values of  $A$  and  $m$  for each data type and mark type, and the value of a single bin below 1 Mpc for each data type and mark type. The significance for the single bin is taken as the distance away from  $M(s) = 1$ , the expected value given no correlation.

Data Type	Mark Type	$A$	$m$	Single Bin Value
(1)	(2)	(3)	(4)	(5)
SAMI Spin Data	Real	$-0.038^{+0.012}_{-0.013}$	$1.060^{+0.196}_{-0.179}$	$0.925 \pm 0.035$
	Random	$-0.008^{+0.005}_{-0.008}$	$1.850^{+0.412}_{-0.317}$	$0.981 \pm 0.038$
SAMI Mass Data	Real	$0.036^{+0.015}_{-0.015}$	$0.713^{+0.320}_{-0.255}$	$1.058 \pm 0.041$
	Random	$-0.003^{+0.009}_{-0.011}$	$0.795^{+0.706}_{-0.512}$	$1.019 \pm 0.039$
Re-sampled EAGLE Spin Data	Real	$-0.020^{+0.003}_{-0.003}$	$0.529^{+0.092}_{-0.094}$	$0.966 \pm 0.008$
	Random	$-0.001^{+0.002}_{-0.003}$	$0.530^{+0.480}_{-0.332}$	$1.000 \pm 0.008$
Re-sampled EAGLE Mass Data	Real	$0.030^{+0.003}_{-0.003}$	$0.488^{+0.045}_{-0.046}$	$1.066 \pm 0.015$
	Random	$-0.003^{+0.003}_{-0.003}$	$0.379^{+0.414}_{-0.225}$	$1.005 \pm 0.015$
Mass Assigned Spin Data, SAMI	Real	$-0.002^{+0.009}_{-0.008}$	$1.035^{+0.807}_{-0.641}$	$0.984 \pm 0.038$
	Random	$-0.014^{+0.011}_{-0.013}$	$0.792^{+0.536}_{-0.412}$	$0.989 \pm 0.038$
No Slow Rotators Spin Data, SAMI	Real	$-0.035^{+0.013}_{-0.014}$	$1.308^{+0.218}_{-0.183}$	$0.937 \pm 0.037$
	Random	$0.005^{+0.014}_{-0.009}$	$0.812^{+0.662}_{-0.460}$	$1.008 \pm 0.041$

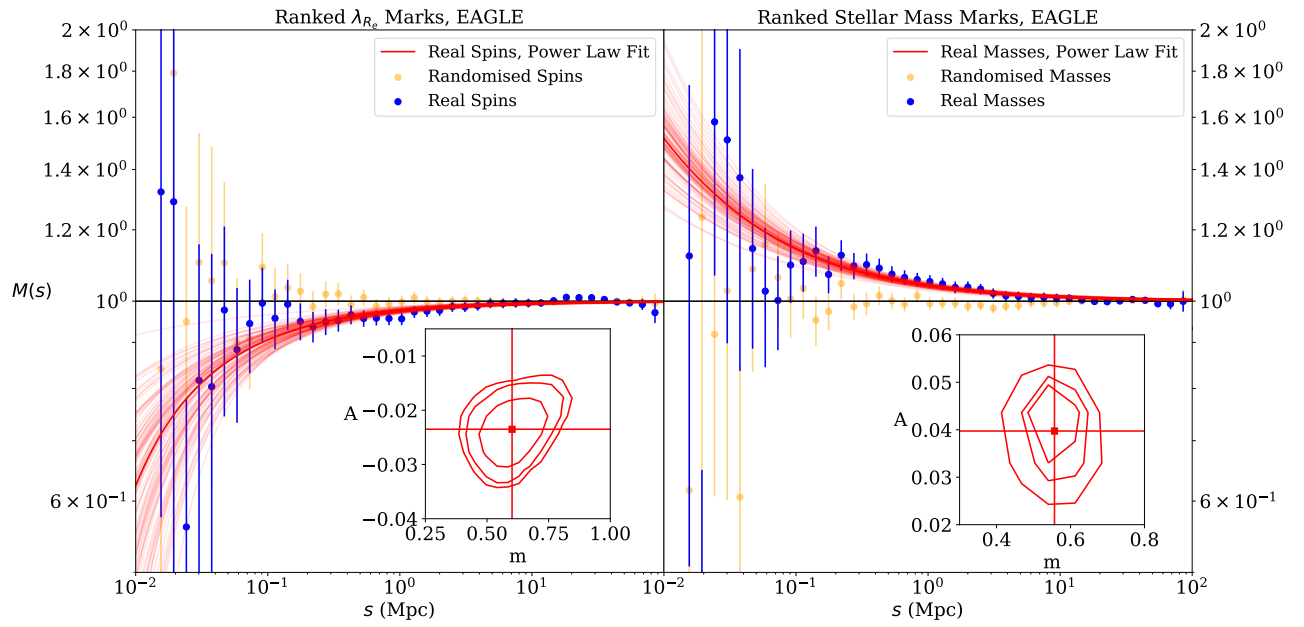


**Figure 4.** Marked correlation functions for ranked  $\lambda_{Re}$  (left panel) and ranked stellar mass marks (right panel). Symbols and lines are similar as in Figure 2, but now presented for the EAGLE data.  $\lambda_{Re}$  is negatively correlated with environment, while stellar mass is positively correlated with environment in EAGLE galaxies.

- The anti-correlation between spin and environment is not driven purely by slow rotators. When slow rotators are removed from the SAMI sample ( $\lambda_{R_e} < 0.2$ ), the anti-correlation is found to still be present.
- Using mock-observations from the EAGLE simulations we find qualitatively consistent results as compared to observed data. Mass is correlated with environment, and spin is anti-correlated with environment with EAGLE galaxies as well as SAMI galaxies. A larger sample size in EAGLE allows us to see to larger scales than SAMI with high signal to noise, but the overall qualitative result remains the same. Although the relationship extends to larger scales for EAGLE, we know there are offsets between SAMI and EAGLE spin values (van de Sande et al. 2019). Investigation of whether these offsets can fully explain the larger scale result is beyond the scope of this paper.

Previous work has suggested that the  $\lambda_{R_e}$ -environment anti-correlation is simply a manifestation of the mass-environment correlation, caused by dynamical friction (Brough et al. 2017; Houghton et al. 2013; Cappellari 2016; Veale et al. 2017; Greene et al. 2017). Our results suggest that the  $\lambda_{R_e}$ -environment anti-correlation is not as simple as a re-statement of the mass-environment correlation. Physical process such as environmental quenching, mergers and interactions may drive galaxies towards lower  $\lambda_{R_e}$  values in denser

environments (see also van de Sande et al., in Prep). The connection between mean stellar population age and environment (e.g. Scott et al. 2017) combined with the relation between mean stellar age and the dynamical thickness or intrinsic shape of galaxies (van de Sande et al. 2018) indicates that the star-formation history of a galaxy, its environment, and dynamical properties are closely connected.

Future IFS surveys such as HECTOR (Bryant et al. 2016) will improve the statistics that we find here, in particular at small separation.

#### ACKNOWLEDGEMENTS

The SAMI Galaxy Survey is based on observations made at the Anglo-Australian Telescope. SAMI was developed jointly by the University of Sydney and the Australian Astronomical Observatory (AAO). The SAMI input catalogue is based on data taken from the Sloan Digital Sky Survey, the GAMA Survey and the VST ATLAS Survey. The SAMI Galaxy Survey is supported by the Australian Research Council (ARC) Centre of Excellence ASTRO 3D (CE170100013) and CAASTRO (CE110001020), and other participating institutions. The SAMI Galaxy Survey website is <http://sami-survey.org/>

JvdS, JJB, JBH, SB, MSO acknowledge support of the ARC (DE200100461, FT180100231, FL140100278, FT140101166, FT140100255). The SAMI instrument was funded by the AAO and JBH through FF0776384, LE130100198. FDE acknowledges funding through the H2020 ERC Consolidator Grant 683184.

#### REFERENCES

- Allen, J. T., Croom, S. M., Konstantopoulos, I. S., et al. 2015, *MNRAS*, 446, 1567, doi: [10.1093/mnras/stu2057](https://doi.org/10.1093/mnras/stu2057)
- Bland-Hawthorn, J., Bryant, J., Robertson, G., et al. 2011, *Optics Express*, 19, 2649, doi: [10.1364/OE.19.002649](https://doi.org/10.1364/OE.19.002649)
- Brough, S., van de Sande, J., Owers, M. S., et al. 2017, 844, 59, doi: [10.3847/1538-4357/aa7a11](https://doi.org/10.3847/1538-4357/aa7a11)
- Bryant, J. J., Bland-Hawthorn, J., Fogarty, L. M. R., Lawrence, J. S., & Croom, S. M. 2014, *MNRAS*, 438, 869, doi: [10.1093/mnras/stt2254](https://doi.org/10.1093/mnras/stt2254)
- Bryant, J. J., Owers, M. S., Robotham, A. S. G., et al. 2015, 447, 2857, doi: [10.1093/mnras/stu2635](https://doi.org/10.1093/mnras/stu2635)
- Bryant, J. J., Bland-Hawthorn, J., Lawrence, J., et al. 2016, in *Society of Photo-Optical Instrumentation Engineers (SPIE) Conference Series*, Vol. 9908, *Ground-based and Airborne Instrumentation for Astronomy VI*, ed. C. J. Evans, L. Simard, & H. Takami, 99081F, doi: [10.1117/12.2230740](https://doi.org/10.1117/12.2230740)
- Bundy, K., Bershady, M. A., Law, D. R., et al. 2015, *ApJ*, 798, 7, doi: [10.1088/0004-637X/798/1/7](https://doi.org/10.1088/0004-637X/798/1/7)
- Cappellari, M. 2016, *ARA&A*, 54, 597, doi: [10.1146/annurev-astro-082214-122432](https://doi.org/10.1146/annurev-astro-082214-122432)
- Cappellari, M., Emsellem, E., Krajnović, D., et al. 2011, 416, 1680, doi: [10.1111/j.1365-2966.2011.18600.x](https://doi.org/10.1111/j.1365-2966.2011.18600.x)
- Choi, H., Yi, S. K., Dubois, Y., et al. 2018, *ApJ*, 856, 114, doi: [10.3847/1538-4357/aab08f](https://doi.org/10.3847/1538-4357/aab08f)
- Croom, S. M., & Shanks, T. 1996, *MNRAS*, 281, 893, doi: [10.1093/mnras/281.3.893](https://doi.org/10.1093/mnras/281.3.893)
- Croom, S. M., Lawrence, J. S., Bland-Hawthorn, J., et al. 2012, 421, 872, doi: [10.1111/j.1365-2966.2011.20365.x](https://doi.org/10.1111/j.1365-2966.2011.20365.x)
- Croom, S. M., Owers, M. S., Scott, N., et al. 2021, *MNRAS*, doi: [10.1093/mnras/stab229](https://doi.org/10.1093/mnras/stab229)
- D'Eugenio, F., Houghton, R. C. W., Davies, R. L., & Dalla Bontà, E. 2013, *MNRAS*, 429, 1258, doi: [10.1093/mnras/sts406](https://doi.org/10.1093/mnras/sts406)

- Dressler, A. 1980, 236, 351, doi: [10.1086/157753](https://doi.org/10.1086/157753)
- Driver, S. P., Hill, D. T., Kelvin, L. S., et al. 2011, 413, 971, doi: [10.1111/j.1365-2966.2010.18188.x](https://doi.org/10.1111/j.1365-2966.2010.18188.x)
- Fisher, K. B., Davis, M., Strauss, M. A., Yahil, A., & Huchra, J. 1994, MNRAS, 266, 50, doi: [10.1093/mnras/266.1.50](https://doi.org/10.1093/mnras/266.1.50)
- Fogarty, L. M. R., Scott, N., Owers, M. S., et al. 2014, MNRAS, 443, 485, doi: [10.1093/mnras/stu1165](https://doi.org/10.1093/mnras/stu1165)
- Foreman-Mackey, D., Hogg, D. W., Lang, D., & Goodman, J. 2013, PASP, 125, 306, doi: [10.1086/670067](https://doi.org/10.1086/670067)
- Graham, M. T., Cappellari, M., Bershad, M. A., & Drory, N. 2019, arXiv e-prints, arXiv:1910.05139. <https://arxiv.org/abs/1910.05139>
- Green, A. W., Croom, S. M., Scott, N., et al. 2018, 475, 716, doi: [10.1093/mnras/stx3135](https://doi.org/10.1093/mnras/stx3135)
- Greene, J. E., Leauthaud, A., Emsellem, E., et al. 2017, ApJL, 851, L33, doi: [10.3847/2041-8213/aa8ace](https://doi.org/10.3847/2041-8213/aa8ace)
- Harborne, K. E., van de Sande, J., Cortese, L., et al. 2020, MNRAS, 497, 2018, doi: [10.1093/mnras/staa1847](https://doi.org/10.1093/mnras/staa1847)
- Harker, G., Cole, S., Helly, J., Frenk, C., & Jenkins, A. 2006, MNRAS, 367, 1039, doi: [10.1111/j.1365-2966.2006.10022.x](https://doi.org/10.1111/j.1365-2966.2006.10022.x)
- Hermit, S., Santiago, B. X., Lahav, O., et al. 1996, 283, 709, doi: [10.1093/mnras/283.2.709](https://doi.org/10.1093/mnras/283.2.709)
- Houghton, R. C. W., Davies, R. L., D'Eugenio, F., et al. 2013, MNRAS, 436, 19, doi: [10.1093/mnras/stt1399](https://doi.org/10.1093/mnras/stt1399)
- Lagos, C. d. P., Schaye, J., Bahé, Y., et al. 2018, 476, 4327, doi: [10.1093/mnras/sty489](https://doi.org/10.1093/mnras/sty489)
- Lagos, C. d. P., Theuns, T., Stevens, A. R. H., et al. 2017, MNRAS, 464, 3850, doi: [10.1093/mnras/stw2610](https://doi.org/10.1093/mnras/stw2610)
- Liske, J., Baldry, I. K., Driver, S. P., et al. 2015, MNRAS, 452, 2087, doi: [10.1093/mnras/stv1436](https://doi.org/10.1093/mnras/stv1436)
- Madgwick, D. S., Hawkins, E., Lahav, O., et al. 2003, 344, 847, doi: [10.1046/j.1365-8711.2003.06861.x](https://doi.org/10.1046/j.1365-8711.2003.06861.x)
- Norberg, P., Baugh, C. M., Hawkins, E., et al. 2001, 328, 64, doi: [10.1046/j.1365-8711.2001.04839.x](https://doi.org/10.1046/j.1365-8711.2001.04839.x)
- . 2002, 332, 827, doi: [10.1046/j.1365-8711.2002.05348.x](https://doi.org/10.1046/j.1365-8711.2002.05348.x)
- Owers, M. S., Allen, J. T., Baldry, I., et al. 2017, 468, 1824, doi: [10.1093/mnras/stx562](https://doi.org/10.1093/mnras/stx562)
- Peebles, P. J. E. 1980, The Large-Scale Structure of the Universe
- Schaye, J., Crain, R. A., Bower, R. G., et al. 2015, MNRAS, 446, 521, doi: [10.1093/mnras/stu2058](https://doi.org/10.1093/mnras/stu2058)
- Scott, N., Davies, R. L., Houghton, R. C. W., et al. 2014, MNRAS, 441, 274, doi: [10.1093/mnras/stu472](https://doi.org/10.1093/mnras/stu472)
- Scott, N., Brough, S., Croom, S. M., et al. 2017, MNRAS, 472, 2833, doi: [10.1093/mnras/stx2166](https://doi.org/10.1093/mnras/stx2166)
- Scott, N., van de Sande, J., Croom, S. M., et al. 2018, MNRAS, 481, 2299, doi: [10.1093/mnras/sty2355](https://doi.org/10.1093/mnras/sty2355)
- Sharp, R., Saunders, W., Smith, G., et al. 2006, in Society of Photo-Optical Instrumentation Engineers (SPIE) Conference Series, Vol. 6269, Society of Photo-Optical Instrumentation Engineers (SPIE) Conference Series, ed. I. S. McLean & M. Iye, 62690G, doi: [10.1117/12.671022](https://doi.org/10.1117/12.671022)
- Sharp, R., Allen, J. T., Fogarty, L. M. R., et al. 2015, MNRAS, 446, 1551, doi: [10.1093/mnras/stu2055](https://doi.org/10.1093/mnras/stu2055)
- Sheth, R. K., Connolly, A. J., & Skibba, R. 2005, arXiv e-prints, astro. <https://arxiv.org/abs/astro-ph/0511773>
- Sheth, R. K., & Tormen, G. 2004, MNRAS, 350, 1385, doi: [10.1111/j.1365-2966.2004.07733.x](https://doi.org/10.1111/j.1365-2966.2004.07733.x)
- van de Sande, J., Bland-Hawthorn, J., Fogarty, L. M. R., et al. 2017a, ApJ, 835, 104, doi: [10.3847/1538-4357/835/1/104](https://doi.org/10.3847/1538-4357/835/1/104)
- van de Sande, J., Bland-Hawthorn, J., Brough, S., et al. 2017b, MNRAS, 472, 1272, doi: [10.1093/mnras/stx1751](https://doi.org/10.1093/mnras/stx1751)
- van de Sande, J., Scott, N., Bland-Hawthorn, J., et al. 2018, Nature Astronomy, 2, 483, doi: [10.1038/s41550-018-0436-x](https://doi.org/10.1038/s41550-018-0436-x)
- van de Sande, J., Lagos, C. D. P., Welker, C., et al. 2019, MNRAS, 484, 869, doi: [10.1093/mnras/sty3506](https://doi.org/10.1093/mnras/sty3506)
- van de Sande, J., Vaughan, S. P., Cortese, L., et al. 2020, arXiv e-prints, arXiv:2011.08199. <https://arxiv.org/abs/2011.08199>
- Veale, M., Ma, C.-P., Greene, J. E., et al. 2017, MNRAS, 471, 1428, doi: [10.1093/mnras/stx1639](https://doi.org/10.1093/mnras/stx1639)
- Veale, M., Ma, C.-P., Thomas, J., et al. 2017, 464, 356, doi: [10.1093/mnras/stw2330](https://doi.org/10.1093/mnras/stw2330)
- Wang, B., Cappellari, M., Peng, Y., & Graham, M. 2020, MNRAS, 495, 1958, doi: [10.1093/mnras/staa1325](https://doi.org/10.1093/mnras/staa1325)
- York, D. G., Adelman, J., Anderson, John E., J., et al. 2000, 120, 1579, doi: [10.1086/301513](https://doi.org/10.1086/301513)